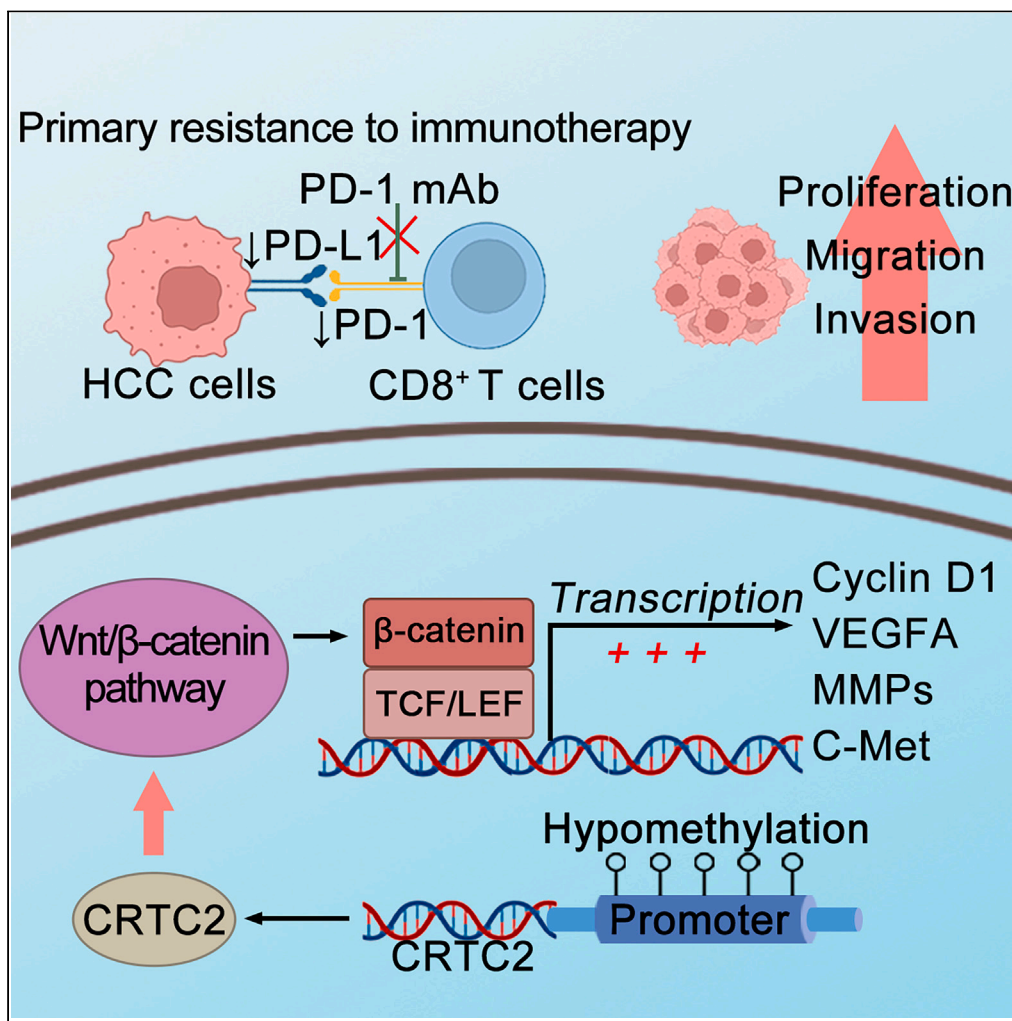Article

Hypomethylation-enhanced CRTC2 expression drives malignant phenotypes and primary resistance to immunotherapy in hepatocellular carcinoma

Ruizhi Zhang, Jingjing Dai, Feifan Yao, ..., Liren Zhang, Jing Xu, Qing Li

15951088290@163.com (J.D.)
bq_fan@139.com (B.F.)
zhangliren@njmu.edu.cn (L.Z.)
xujing7901@jsph.org.cn (J.X.)
liqingjsph@njmu.edu.cn (Q.L.)

Highlights

DNA hypomethylation is responsible for the upregulation of *CRTC2* in HCC

CRTC2 promotes HCC malignant phenotypes by activating the Wnt/β-catenin pathway

CRTC2 downregulates the PD-L1/PD-1 axis

Targeting *CRTC2* improves the efficacy of anti-PD-1 immunotherapy in HCC

iScience

Article

Hypomethylation-enhanced CRTC2 expression drives malignant phenotypes and primary resistance to immunotherapy in hepatocellular carcinoma

Ruizhi Zhang,[1,8] Jingjing Dai,[2,8,*] Feifan Yao,[1,8] Suiqing Zhou,[1,8] Wei Huang,[3,8] Jiali Xu,[4,8] Kai Yu,[1] Yining Chen,[5] Boqiang Fan,[6,*] Liren Zhang,[1,*] Jing Xu,[6,*] and Qing Li[1,7,9,*]

SUMMARY

The cyclic AMP-responsive element-binding protein (CREB)-regulated transcription coactivator 2 (CRTC2) is a crucial regulator of hepatic lipid metabolism and gluconeogenesis and correlates with tumorigenesis. However, the mechanism through which CRTC2 regulates hepatocellular carcinoma (HCC) progression is largely unknown. Here, we found that increased CRTC2 expression predicted advanced tumor grade and stage, as well as worse prognosis in patients with HCC. DNA promoter hypomethylation led to higher *CRTC2* expression in HCC. Functionally, *CRTC2* contributed to HCC malignant phenotypes through the activated Wnt/β-catenin pathway, which could be abrogated by the small-molecular inhibitor XAV-939. Moreover, *Crtc2* facilitated tumor growth while concurrently downregulating the PD-L1/PD-1 axis, resulting in primary resistance to immunotherapy. In immunocompetent mice models of HCC, targeting *Crtc2* in combination with anti-PD-1 therapy prominently suppressed tumor growth by synergistically enhancing responsiveness to immunotherapy. Collectively, targeting *CRTC2* might be a promising therapeutic strategy to sensitize immunotherapy in HCC.

INTRODUCTION

Hepatocellular carcinoma (HCC), one of the most commonly diagnosed forms of primary liver malignancy, has high morbidity and mortality rates worldwide.[1–5] HCC usually originates from cirrhosis induced by chronic inflammatory infections, such as hepatitis virus infection, especially hepatitis B virus (HBV) in China, and is closely associated with excessive alcohol consumption and steatohepatitis related to obesity and metabolic syndrome.[1,2,5] Although HCC treatments have witnessed significant progress in surgery, local ablation, and emerging immunotherapy strategies over the last few decades, the prognosis of patients with HCC is still poorly improved, with a minimal 5-year overall survival (OS).[6–10] Surgical interventions, such as hepatectomy and liver transplantation, have been shown to significantly improve the 5-year survival rate for patients diagnosed with early-stage HCC.[11] However, when seeking consultation, most patients with HCC are already at advanced stages owing to atypical early symptoms, distant metastases, and rapid disease development, thus precluding curative surgical resection. Although treatments for patients with advanced HCC are limited, promising advances have been made in therapies based on molecularly targeted drugs including immune checkpoint inhibitors (ICIs) and multi-kinase inhibitors (TKIs). ICIs exhibit antitumor effects by blocking the interaction between checkpoint proteins and their ligands and activating the antitumor effect of tumor-infiltrating T cells.[7,12–14] TKIs exhibit antitumor and anti-angiogenesis effects by downregulating the kinase activity of Ras/Raf/MEK/ERK signaling pathways and targeting proteins involved in angiogenesis.[15–17] However, the efficacy of these medications is restricted in that they only prolong the lifespan of patients with HCC by 2–3 months with low response rates or induce drug resistance, which finally leads to treatment failure and tumor recurrence.[18–20] Therefore, a better understanding of HCC malignancy may lead to more efficient treatment strategies.

With the presence of CREB-regulated transcription coactivators (CRTCs), the transcription factor CREB modulates multiple cellular communications in response to a range of extracellular signals, by interacting with cyclic AMP (cAMP) response elements containing genes.[21,22] The CRTC family consists of three members namely CRTC1, CRTC2, and CRTC3. CRTC2 is prevalent in the liver and controls the

[1]Hepatobiliary Center, The First Affiliated Hospital of Nanjing Medical University, Key Laboratory of Liver Transplantation, Chinese Academy of Medical Sciences, NHC Key Laboratory of Hepatobiliary Cancers, Nanjing, Jiangsu Province 210000, China
[2]Department of Infectious Diseases, The First Affiliated Hospital of Nanjing Medical University, Nanjing, Jiangsu Province 210000, China
[3]Department of General Surgery, The Friendship Hospital of Ili Kazakh Autonomous Prefecture, Ili & Jiangsu Joint Institute of Health, Ili 835000, China
[4]Department of Anesthesiology, Jinling Hospital, Affiliated Hospital of Medical School, Nanjing University, Nanjing, Jiangsu Province 210000, China
[5]Department of Anesthesiology and Perioperative Medicine, The First Affiliated Hospital of Nanjing Medical University, Nanjing, Jiangsu Province 210000, China
[6]Department of Oncology, The First Affiliated Hospital of Nanjing Medical University, Nanjing, Jiangsu Province 210000, China
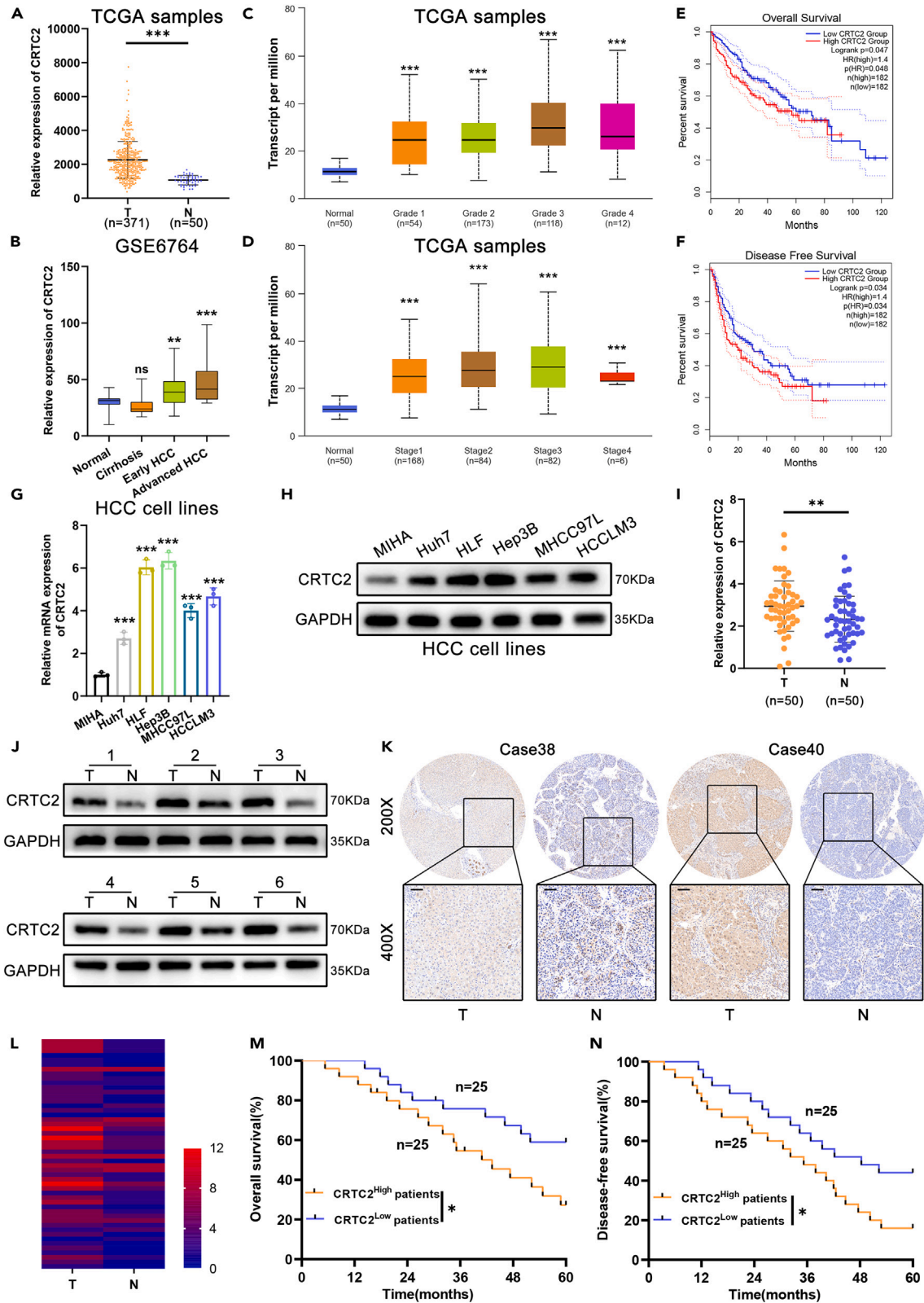[7]Collaborative Innovation Center for Cancer Personalized Medicine, Nanjing Medical University, Nanjing, Jiangsu Province 210000, China
[8]These authors contributed equally
[9]Lead contact
*Correspondence: 15951088290@163.com (J.D.), bq_fan@139.com (B.F.), zhangliren@njmu.edu.cn (L.Z.), xujing7901@jsph.org.cn (J.X.), liqingjsph@njmu.edu.cn (Q.L.)
https://doi.org/10.1016/j.isci.2024.109821

Figure 1. CRTC2 is overexpressed in HCC and correlated with poor prognosis

(A) Dot plot showing the mRNA expression levels of *CRTC2* in HCC tissues compared to normal liver tissues from the TCGA database.

(B) Dot plots demonstrating stage-dependent expression of *CRTC2* during HCC progression in the GSE6764 dataset.

(C and D) Upregulated *CRTC2* mRNA expression was significantly associated with patient tumor grade and stage in HCC. Tumor grade information was not available for 14 samples and undetermined for 5 samples. Cancer stage information was not available for 31 samples.

(E and F) Kaplan-Meier analysis showing the overall survival and disease-free survival of patients with diverse CRTC2 expression.

(G and H) The levels of CRTC2 mRNA and protein expression in normal liver cell line and HCC cell lines.

(I) *CRTC2* mRNA expression was detected in 50 paired HCC tissues and matched adjacent normal tissues.

(J) Protein expression of CRTC2 was detected in 6 paired HCC tissues and matched adjacent normal tissues. GAPDH was used for normalization.

(K and L) Representative images of CRTC2 expression in paired HCC specimens and IHC analysis, *n* = 50 per group, scale bars, 50 μm.

(M and N) Survival analysis using the Kaplan-Meier method after dividing patients with HCC into the low or high CRTC2 expression groups, *n* = 25 per group. All data are presented as the means ± SD, **p < 0.01; ***p < 0.001; ns, not significant.

transcriptional activity of hepatic gluconeogenesis-related genes with the assistance of CREB.[23–25] CRTC2 hepatic depletion effectively ameliorates nonalcoholic steatohepatitis progression by reducing lipid accumulation.[26] Recently, numerous studies have explored the potential role of CRTC2 in malignancies, including lymphoma, lung cancer, prostate cancer, and colorectal cancer.[27–30] For example, when phosphorylated at Ser238, CRTC2 promotes colorectal cancer progression.[30] In prostate cancer, high CRTC2 expression has been identified as a prognostic factor of postoperative biochemical recurrence.[29] In lymphoma, CRTC2 confers tumor suppression by promoting the transcriptional activity of DNA mismatch repair genes to preserve genome integrity.[27] However, the mechanism by which CRTC2 regulates HCC progression remains unknown.

In this study, we found that increased CRTC2 expression predicts poor prognosis in patients with HCC. *CRTC2* upregulation is attributed to DNA promoter hypomethylation. *CRTC2* facilitates HCC malignant phenotypes by upregulating the Wnt/β-catenin pathway and drives primary resistance to immunotherapy by downregulating the PD-L1/PD-1 axis. In immunocompetent mice models of HCC, targeting *Crtc2* in combination with anti-PD-1 therapy prominently suppressed tumor growth by synergistically enhancing responsiveness to immunotherapy. Collectively, targeting *CRTC2* might be a promising therapeutic strategy to sensitize immunotherapy in HCC.

RESULTS

Increased CRTC2 expression indicates poor prognosis in patients with HCC

By analyzing The Cancer Genome Atlas (TCGA) Liver hepatocellular carcinoma (LIHC) cohort, we identified a substantial upregulation of *CRTC2* mRNA expression in HCC tissues as compared to normal liver tissues (Figure 1A). Elevated *CRTC2* mRNA expression was also observed in patients with early and advanced HCC in the GSE6764 database, which confirmed that *CRTC2* expression was upregulated in HCC in a stage-dependent manner (Figure 1B). In the UALCAN database, patients with HCC of grades 1, 2, 3, and 4 showed progressively elevated *CRTC2* expression (Figure 1C). *CRTC2* expression was also progressively elevated at stages 1, 2, 3, and 4, suggesting that its expression may be an indicator of HCC progression (Figure 1D). In addition, we conducted survival analysis based on Gene Expression Profiling Interactive Analysis (GEPIA) database, and our findings indicated that patients with higher *CRTC2* mRNA expression displayed unfavorable OS and disease-free survival (DFS) in HCC (Figures 1E and 1F). In addition to our findings in clinical samples, the mRNA and protein levels of CRTC2 were significantly higher in HCC cell lines compared to immortalized liver cell line MIHA. Among the HCC cell lines, Hep3B and Huh7 cells had the relatively higher and lower mRNA and protein levels of CRTC2, respectively (Figures 1G and 1H). To expand our investigation, we collected 50 pairs of HCC tissues and matched adjacent normal tissues and found that the mRNA expression of *CRTC2* was considerably upregulated in the HCC tissues compared to the matched adjacent normal tissues (Figure 1I). We randomly selected six pairs of HCC specimens to examine CRTC2 protein expression in HCC tissues. CRTC2 protein expression was significantly increased in HCC tissues as compared to the matched adjacent normal tissues (Figure 1J). The results of immunohistochemistry (IHC) staining showed a significant increase in the IHC staining score of CRTC2 in tumor tissues compared to the matched adjacent normal tissues (Figures 1K and 1L). Meanwhile, patients with high CRTC2 expression had reduced OS and DFS (Figures 1M and 1N). Additionally, clinicopathological examination (Tables S1 and S2) revealed that increased CRTC2 expression was significantly correlated with larger tumor size (*p* = 0.024), presence of microvascular invasion (*p* = 0.004), incomplete tumor encapsulation (*p* = 0.023), and advanced Edmonson stages (*p* = 0.009). Collectively, these findings suggested that CRTC2 is overexpressed in HCC and increased CRTC2 expression predicts poor prognosis in patients with HCC.

### *CRTC2* upregulation is attributed to DNA promoter hypomethylation

The bioinformatic analysis indicated that CRTC2 promoter region contains a typical CpG island, suggesting that DNA promoter hypomethylation may contribute to *CRTC2* upregulation in HCC (Figure 2A). Analysis based on the cBioPortal database revealed that *CRTC2* mRNA expression was negatively associated with the DNA methylation level (Pearson correlation coefficient: −0.39; *p* = 2.72e−15; Figure 2B). We exposed Hep3B cells, which exhibit relatively higher CRTC2 expression, and Huh7 cells, which display relatively lower CRTC2 expression, to 5-aza-2′-deoxycytidine (5-Aza-dC), a widely used DNA methyltransferase inhibitor. Methylation-specific PCR (MSP) results indicated that 5-Aza-dC significantly inhibited DNA methylation levels of CRTC2 promoter sequence (Figure 2C). In comparison to cells not treated with 5-Aza-dC, HCC cells exposed to 5-Aza-dC exhibited a notable upregulation in *CRTC2* mRNA expression, suggesting a negative correlation between *CRTC2* mRNA expression and DNA methylation levels (Figure 2D). A recent study has shown that DNA
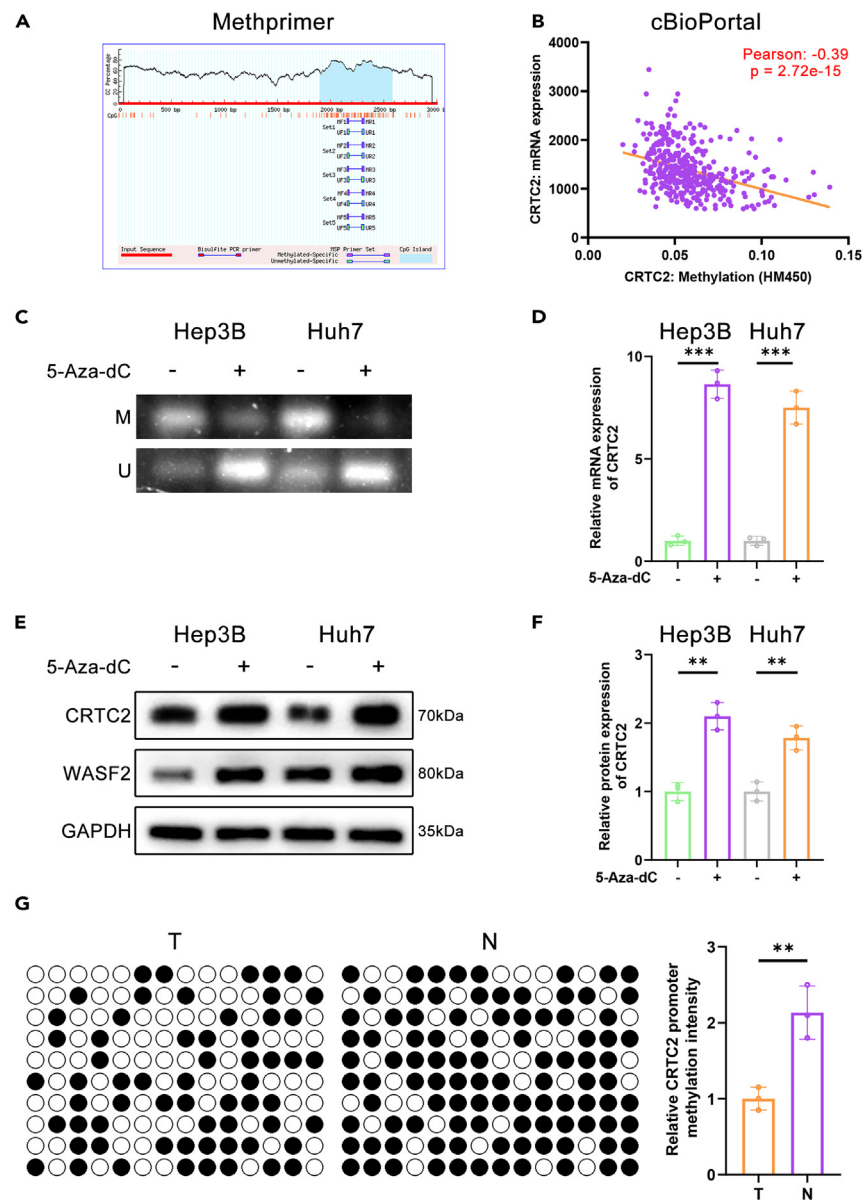
Figure 2. *CRTC2* upregulation in HCC is attributed to DNA hypomethylation

(A) The online bioinformatic tool was utilized to screen the possible CpG islands in CRTC2 promoter sequence.

(B) The cBioPortal database was employed to analyze the association between DNA methylation level and *CRTC2* mRNA expression in HCC.

(C) DNA methylation level in HCC cells as determined using methylation-specific PCR (MSP); M, methylation; U, unmethylation.

(D) The expression of *CRTC2* mRNA was evaluated in Hep3B and Huh7 cells after 5-Aza-dC treatment.

(E and F) Detection and quantitation of CRTC2 protein expression in Hep3B and Huh7 cells after 5-Aza-dC treatment.

(G) The DNA methylation status of CRTC2 CpG islands in three randomly chosen HCC tissues and matched adjacent normal tissues as determined by bisulfite sequencing PCR (BSP). Unmethylated CpG sites were represented by open circles, while methylated CpG sites were indicated by filled circles. $n = 3$ per group. All data are presented as the means $\pm$ SD of three independent experiments, $**p < 0.01$; $***p < 0.001$.

promoter hypomethylation upregulates WASF2 expression in HCC.[31] Therefore, we chose WASF2 as a marker to ascertain the effect of 5-Aza-dC treatment (Figure 2E). Following treatment with 5-Aza-dC, we detected and quantified CRTC2 protein expression in HCC cells. The results demonstrated that HCC cells incubated with 5-Aza-dC exhibited an increase in CRTC2 protein expression level (Figures 2E and 2F). Moreover, bisulfite sequencing PCR (BSP) results suggested that the CRTC2 DNA promoter sequence was hypomethylated in tumors compared with adjacent normal tissues (Figure 2G). Taken together, our findings suggested that *CRTC2* upregulation in HCC can be attributed to DNA promoter hypomethylation.
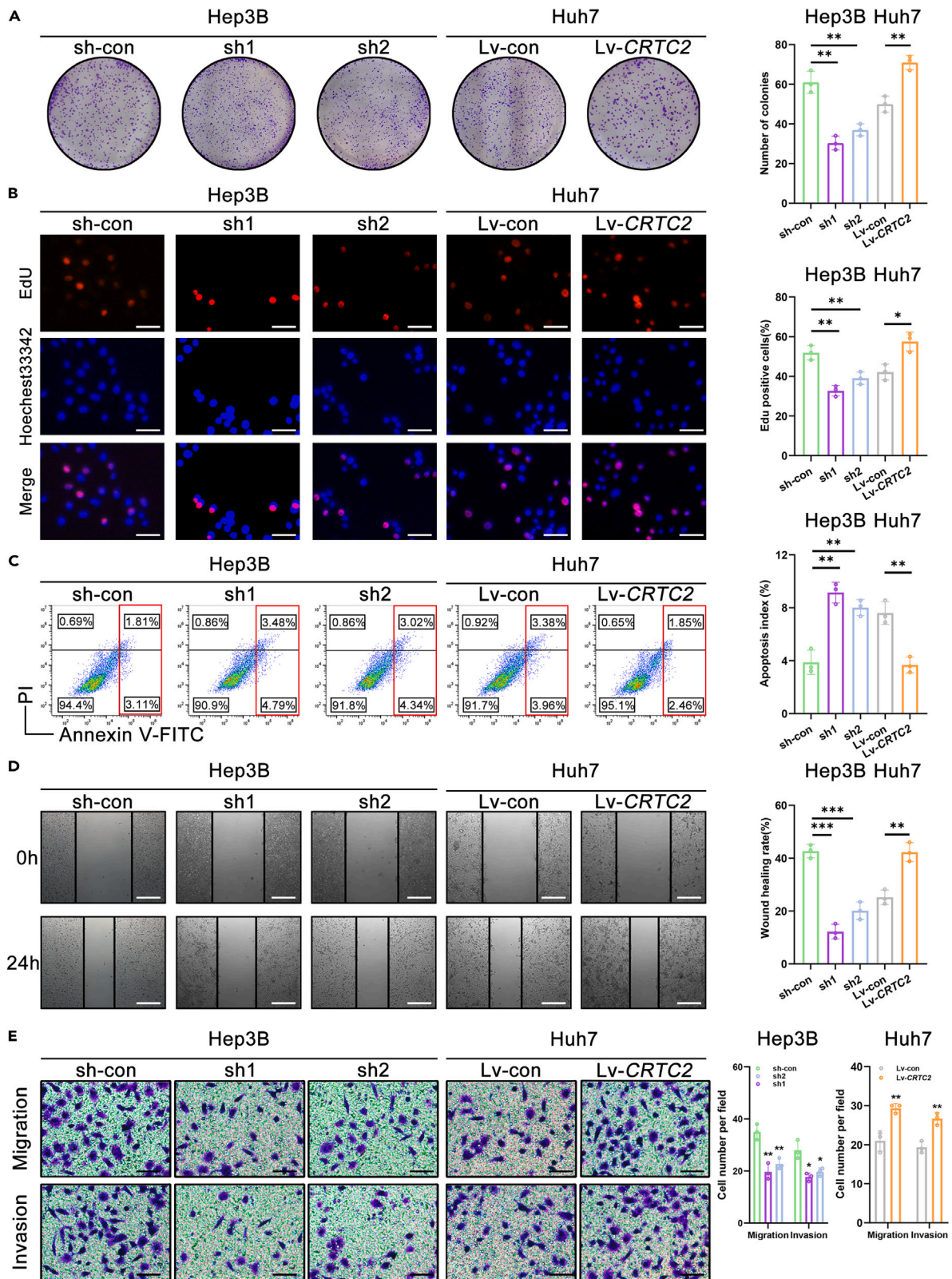
Figure 3. *CRTC2* drives HCC malignant phenotypes *in vitro*

(A) Colony formation assays were carried out to evaluate the impact of *CRTC2* knockdown or overexpression on HCC cell proliferation.

(B) EdU assays were utilized to determine the impact of *CRTC2* knockdown or overexpression on the proliferation of HCC cells (scale bars, 50 μm).

(C) Flow cytometry assays were used to assess the effect of *CRTC2* knockdown or overexpression on cell apoptosis.

(D) The effects of *CRTC2* knockdown or overexpression on HCC cell migration as evaluated by wound healing assays (scale bars, 200 μm).

(E) Transwell assays were used to evaluate the migration and invasion of transfected HCC cells (scale bars, 50 μm). All data are presented as the means ± SD of three independent experiments, *$p < 0.05$; **$p < 0.01$; ***$p < 0.001$.

CRTC2 facilitates HCC malignant phenotypes both *in vitro* and *in vivo*

To further explore the role of CRTC2 in HCC, Hep3B cells were infected with short hairpin RNA (shRNA)-mediated CRTC2 knockdown (sh1, sh2, and sh3), and Huh7 cells were infected with lentivirus-mediated CRTC2 overexpression (Lv-*CRTC2*). Then we validated the transfection efficiency in each group. Both sh1 and sh2 exhibited apparent inhibition in Hep3B cells and were selected for further functional experiments (Figures S1A and S1B). The results of Cell Counting Kit-8 (CCK-8) assays, colony formation assays, and 5′-ethynyl-2′-deoxyuridine (EDU) assays affirmed that *CRTC2* knockdown impeded cell proliferation, whereas *CRTC2* overexpression promoted cell proliferation (Figures S2A, S2B, 3A, and 3B). Moreover, flow cytometry analysis revealed that *CRTC2* knockdown increased the ratio of apoptotic cells, while *CRTC2* overexpression mitigated cell apoptosis (Figure 3C). We conducted wound healing and transwell assays to evaluate the impact of *CRTC2* dysregulation on cell migration and invasion. The results demonstrated a substantial inhibition of cell migration and invasion following *CRTC2* knockdown. Contrary to the effect of *CRTC2* knockdown, *CRTC2* overexpression dramatically promoted the malignant phenotypes of HCC cells (Figures 3D and 3E). Collectively, our findings confirmed that *CRTC2* facilitates HCC malignant phenotypes *in vitro*.

To assess the influence of CRTC2 on HCC malignant phenotypes *in vivo*, transfected HCC cells were subcutaneously injected into nude mice. *CRTC2* knockdown suppressed tumor growth and reduced tumor size in comparison with the control group (Figures 4A, 4B, and 4C). Meanwhile, *CRTC2* overexpression promoted tumor growth and increased tumor size as compared to the control group (Figures 4D, 4E, and 4F). As determined by IHC staining, *CRTC2* knockdown inhibited the proliferation of HCC cells and increased apoptosis rate, whereas *CRTC2* overexpression facilitated the proliferation of HCC cells and decreased apoptosis (Figure 4G). In lung metastatic model, *CRTC2* knockdown group had less tumor metastasis, while *CRTC2* overexpression group showed a higher incidence of tumor metastasis, as indicated by bioluminescence analysis (Figures 4H and 4I). In addition, survival analysis revealed that *CRTC2* knockdown group displayed prolonged OS, whereas the *CRTC2* overexpression group exhibited reduced OS (Figures 4J and 4K). Taken together, our results indicated that *CRTC2* facilitates HCC malignant phenotypes both *in vitro* and *in vivo*.

CRTC2 drives HCC malignant phenotypes by activating the Wnt/β-catenin pathway

To illustrate the possible molecular mechanisms by which CRTC2 confers its effects in promoting HCC malignant phenotypes, we conducted RNA sequencing analysis in Huh7 Lv-con cells and Lv-*CRTC2* cells to identify the differently expressed genes (Figure 5A). The genes whose expression was upregulated over 2.0-fold in *CRTC2*-overexpressing Huh7 cells were identified to conduct the pathway enrichment analysis. Kyoto Encyclopedia of Genes and Genomes (KEGG) pathway analysis suggested that *CRTC2* overexpression affected multiple signaling pathways that contribute to inflammation, cancer, and metabolism, among which the Wnt/β-catenin pathway had the highest correlation with CRTC2 (Figure 5B). Substantial research has been conducted to elucidate the oncogenic role of Wnt/β-catenin pathway in HCC.[32,33] Thus, we speculated that CRTC2 may play a critical role in regulating Wnt/β-catenin pathway. The downstream target protein expression of the Wnt/β-catenin pathway was detected in stably transfected HCC cells. We found that protein levels of β-catenin, cyclinD1, CD44, c-Met, c-Jun, and TCF-1 were significantly decreased in the *CRTC2*-knockdown group, but increased in the *CRTC2*-overexpression group (Figure 5C). We further conducted dual luciferase reporter assays to validate the transcriptional activity of Wnt/β-catenin pathway in transfected HCC cells. The results suggested that *CRTC2* knockdown considerably decreased the transcriptional activity of T cell factor (TCF)/lymphoid enhancer factor (LEF), while *CRTC2* overexpression led to opposite results (Figure 5D). The compound XAV-939, known for its inhibitory effect on the Wnt/β-catenin pathway by targeting tankyrase, was utilized to validate whether *CRTC2* promotes malignant phenotypes in HCC through the activated Wnt/β-catenin pathway.[34] The downstream target protein expression of the Wnt/β-catenin pathway was significantly increased in the *CRTC2*-overexpression group as compared to the control group (Figure 6A). Notably, XAV-939 treatment restrained the downstream target protein expression of the Wnt/β-catenin pathway in Huh7 Lv-*CRTC2* cells (Figure 6A). The dual luciferase reporter assays validated that XAV-939 inhibited the transcriptional activity of TEF/LCF in the *CRTC2*-overexpression group (Figure 6B). Additionally, we found that XAV-939 treatment significantly reversed the malignant phenotypes of HCC cells induced by *CRTC2* overexpression (Figures 6C–6F). Taken together, these findings confirmed that *CRTC2* overexpression drives HCC malignant phenotypes by activating the Wnt/β-catenin pathway.

Crtc2 downregulates the PD-L1/PD-1 axis

To comprehensively investigate the impact of CRTC2 on tumor microenvironment, we established the immunocompetent subcutaneous tumor model using H22 Lv-vector and Lv-*Crtc2* cells. Tumors from each group were isolated, and overall changes in the immune cells were analyzed by mass cytometry. All specimens were clustered and annotated under the common immune cell marker CD45⁺. Based on unique markers for each cell type, we identified 27 cell populations separately (Figures 7A–7C). *Crtc2* overexpression significantly reduced the infiltration of PD-1⁺ immune cells compared to the control group (Figures 7D and 7E). Thus, we supposed that *Crtc2* may downregulate the
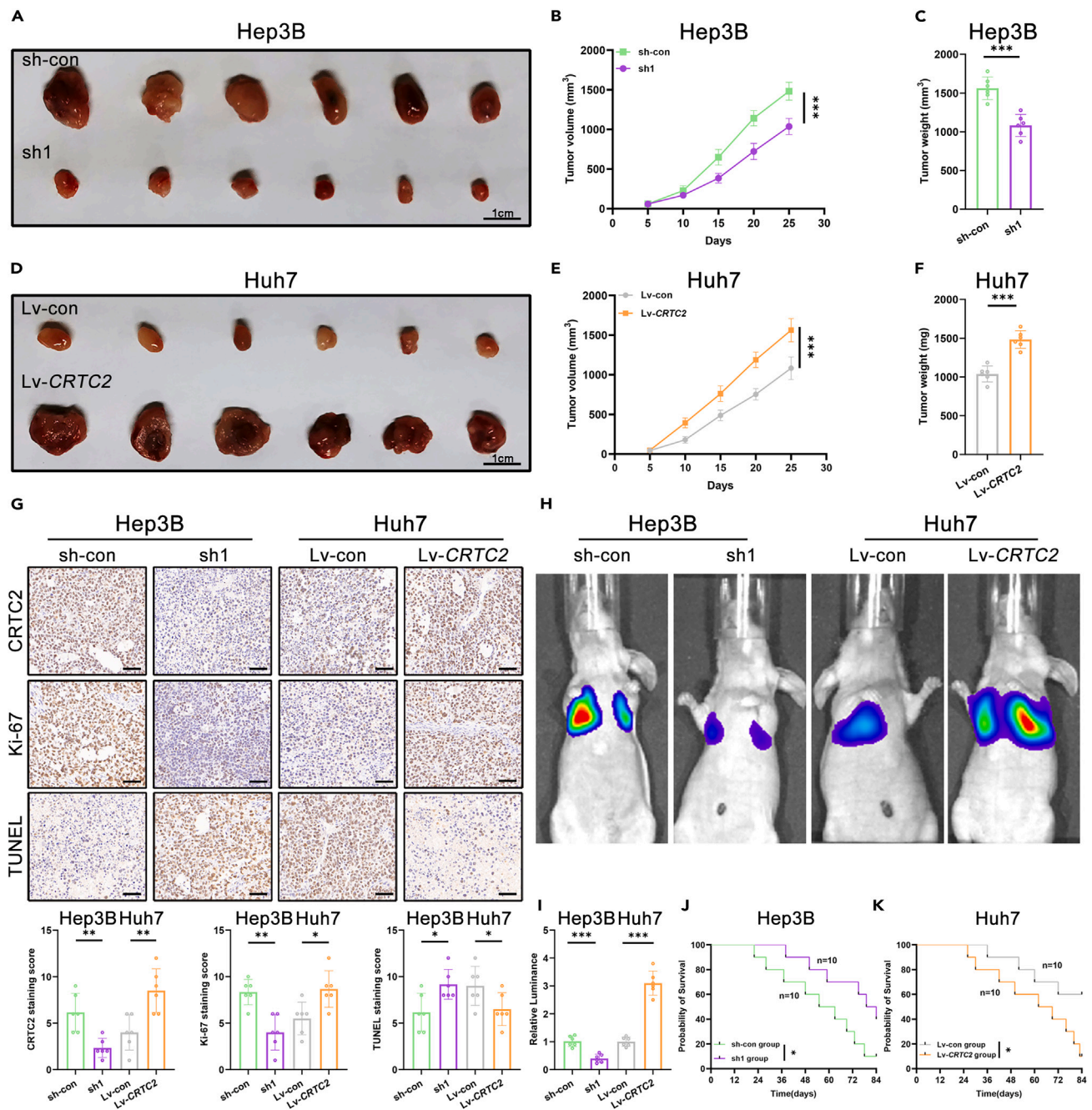
Figure 4. *CRTC2* facilitates HCC growth and metastasis *in vivo*

(A) Four weeks after subcutaneous injections of *CRTC2*-knockdown cells into nude mice, the tumors were isolated for analysis.

(B and C) The size and weight of subcutaneous tumors, $n = 6$ per group.

(D) Four weeks after subcutaneous injections of *CRTC2*-overexpression cells into nude mice, the tumors were isolated for analysis.

(E and F) The size and weight of subcutaneous tumors, $n = 6$ per group.

(G) Representative CRTC2, Ki-67, and TUNEL immunostaining of subcutaneous tumors (scale bars, 100 μm), and the quantitation of immunohistochemical staining score was shown, $n = 6$ per group.

(H and I) Bioluminescence images of lung metastasis model and the quantitation of the corresponding luciferase activity were shown, $n = 6$ per group.

(J and K) Survival analysis of the lung metastasis model in each group, $n = 10$ per group. All data are presented as the means ± SD, *$p < 0.05$; **$p < 0.01$; ***$p < 0.001$.
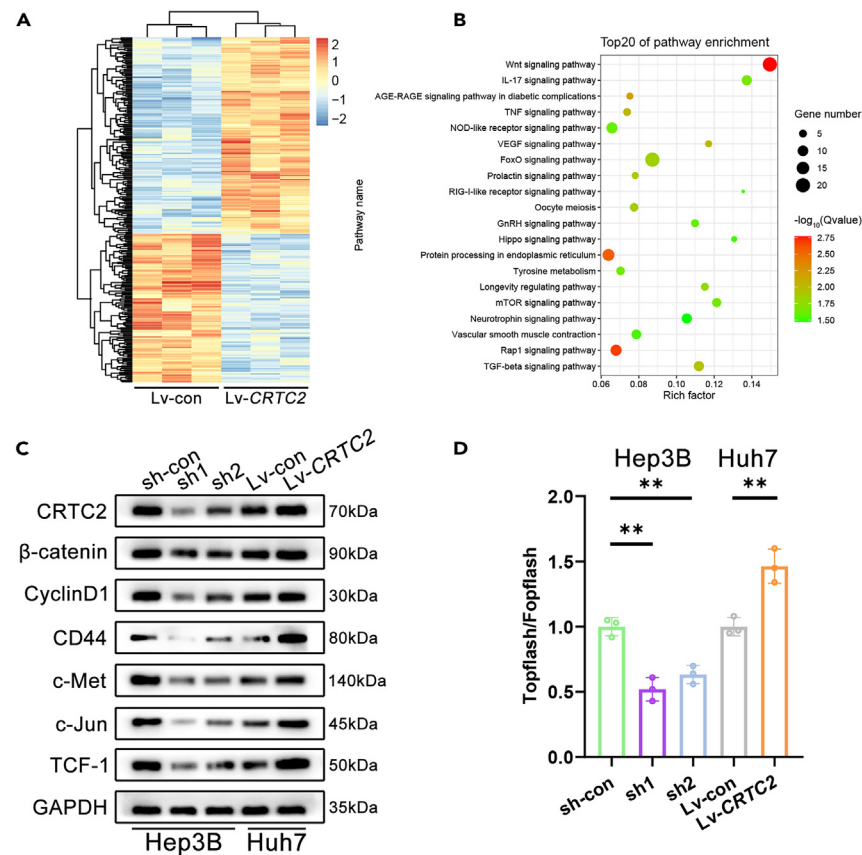
Figure 5. *CRTC2* overexpression activates the Wnt/β-catenin pathway in HCC
(A) Heatmap showing changes in gene expression after *CRTC2* upregulation.
(B) Top 20 pathways of KEGG enrichment analysis.
(C) Protein levels of β-catenin, cyclinD1, CD44, c-Met, c-Jun, and TCF-1 in HCC cells following *CRTC2* knockdown or overexpression.
(D) The dual luciferase reporter assay was conducted to analyze the transcriptional activity of TCF/LEF in transfected HCC cells. All data are presented as the means ± SD of three independent experiments, **$p < 0.01$.

PD-L1/PD-1 axis. We further detected the PD-L1 protein expression in transfected human HCC cells. The results suggested that *CRTC2* knockdown upregulated PD-L1 protein expression, while *CRTC2* overexpression downregulated PD-L1 protein expression (Figure 7F). Similarly, *Crtc2* knockdown also upregulated PD-L1 protein expression in mouse HCC cells (Figure 7G). We further established orthotopic models to confirm the aforementioned findings *in vivo*. *Crtc2* overexpression led to larger tumor size, increased tumor-infiltrating CD8+ T cells, and downregulated the proportion of exhausted CD8+ PD-1+ T cells in comparison with the control group (Figures 7H–7M). Collectively, these findings suggested that *Crtc2* facilitates tumor growth, downregulates the PD-L1/PD-1 axis, and increases the infiltration of CD8+ T cells.

Targeting *Crtc2* sensitizes anti-PD-1 therapy in HCC

As *Crtc2* downregulates the PD-L1/PD-1 axis, we hypothesized that targeting *Crtc2* may synergize with anti-PD-1 therapy in HCC progression. To test this hypothesis, we established subcutaneous and orthotopic models of HCC to explore the therapeutic effect of anti-PD-1 in combination with *Crtc2* knockdown. The mice were treated with either anti-PD-1 or immunoglobulin G (IgG) isotype following the schematic schedule (Figures 8A and 8G). As revealed by gross appearance, *Crtc2*-knockdown treatment inhibited both subcutaneous and orthotopic tumor growth compared to the control group (Figures 8B–8E and 8H–8K). Importantly, the combination therapy of *Crtc2* knockdown and anti-PD-1 resulted in significantly restrained tumor growth in comparison with *Crtc2*-knockdown treatment alone (Figures 8B–8E and 8H–8K). Flow cytometry analysis confirmed that *Crtc2*-knockdown treatment decreased the tumor-infiltrating CD8+ T cells and upregulated the proportion of exhausted CD8+ PD-1+ T cells, whereas the combination therapy significantly increased the tumor-infiltrating CD8+ T cells and downregulated the proportion of exhausted CD8+ PD-1+ T cells in comparison with *Crtc2*-knockdown treatment alone (Figures 8F and 8L). Further, lysates of orthotopic tumors were collected and determined by ELISA. *Crtc2*-knockdown treatment downregulated the levels of immunostimulatory cytokines tumor necrosis factor alpha (TNF-α) and interferon (IFN)-γ and upregulated those of immunosuppressive cytokines
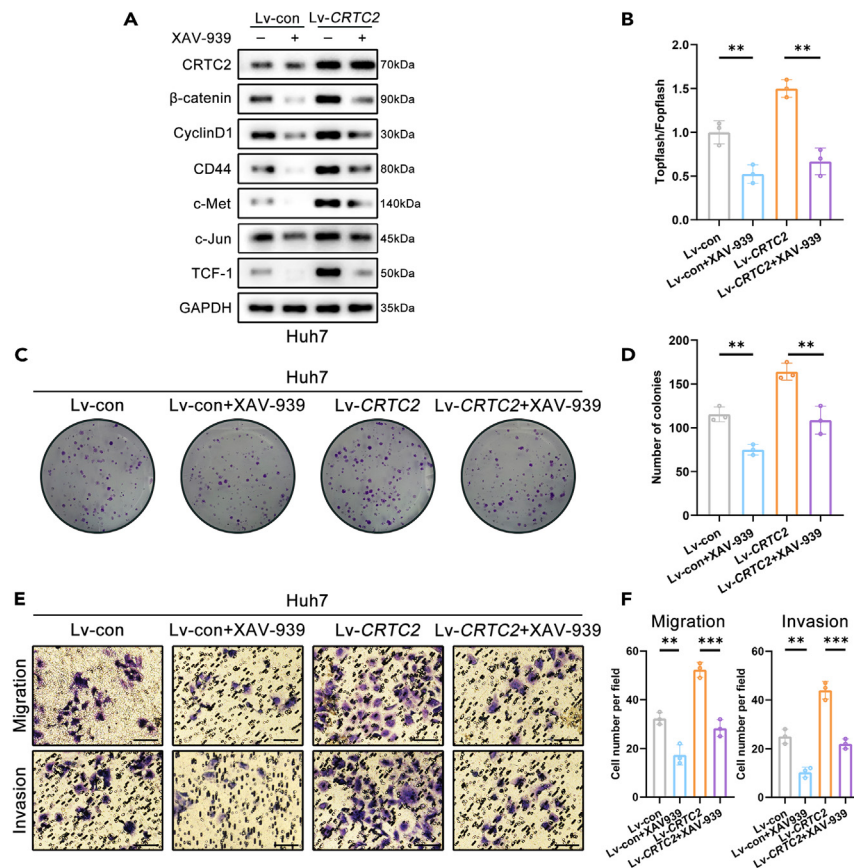
Figure 6. Inhibition of the Wnt/β-catenin pathway suppresses CRTC2-induced promotion of HCC malignant phenotypes

(A) Western blot analysis of β-catenin, cyclinD1, CD44, c-Met, c-Jun, and TCF-1 in the transfected Huh7 cells exposed or unexposed to XAV-939.

(B) The dual luciferase reporter assay was conducted to assess the transcriptional activity of TCF/LEF.

(C and D) Cell proliferation was determined using colony formation assays.

(E and F) Transwell assays were used to measure the migration and invasion of transfected Huh7 cells exposed or unexposed to XAV-939 (scale bars, 50 μm). All data are presented as the means ± SD of three independent experiments, **$p < 0.01$; ***$p < 0.001$.

transforming growth factor β (TGF-β) and interleukin (IL)-10 compared to the control group (Figures S3A–S3D and S3E–S3H). Furthermore, the combination therapy upregulated the levels of TNF-α and IFN-γ and downregulated those of TGF-β and IL-10 as compared to *Crtc2*-knockdown treatment alone (Figures S3A–S3D and S3E–S3H). These findings suggested that combination immunotherapy of targeting *Crtc2* and anti-PD-1 may elicit a more effective antitumor response.

DISCUSSION

As the most commonly diagnosed histological type of primary liver malignancy, HCC poses a substantial threat to human health and is currently the third leading cause of cancer-related deaths worldwide.[1–5] Most patients with HCC are already at advanced stages when seeking consultation and are not suitable for currently available treatments. Hence, elucidation of mechanisms underlying the progression of HCC and identification of therapeutic targets is essential. As the main coactivator of CREB, CRTC2 controls the transcriptional activity of hepatic gluconeogenesis-related genes.[24–26] Recently, numerous studies have explored the potential role of CRTC2 in malignancies.[27–30] In this study, we showed that increased CRTC2 expression predicts poor clinical outcomes in patients with HCC.

DNA promoter methylation is a crucial mechanism in regulating epigenetic modification that controls gene expression during development and disease. During carcinogenesis, aberrant DNA promoter methylation contributes to the development of various genetic disorders.[35,36] Moreover, it was recently reported that hypomethylated DNA promoters play a vital role in the upregulation of certain oncogenes.[8,31] We hypothesized that upregulation of CRTC2 in HCC tissues is associated with DNA methylation. Our results showed that hypomethylation of the CRTC2 promoter drives *CRTC2* upregulation in HCC.

We used RNA sequencing analysis and western blotting to clarify the potential mechanism by which CRTC2 promotes HCC progression and found that the oncogenic effect of CRTC2 was dependent on the Wnt/β-catenin pathway. Once abnormally activated, β-catenin detaches from the complex of Axin, adenomatous polyposis coli (APC), and GSK3β and translocates to the nucleus. β-catenin then binds coactivators
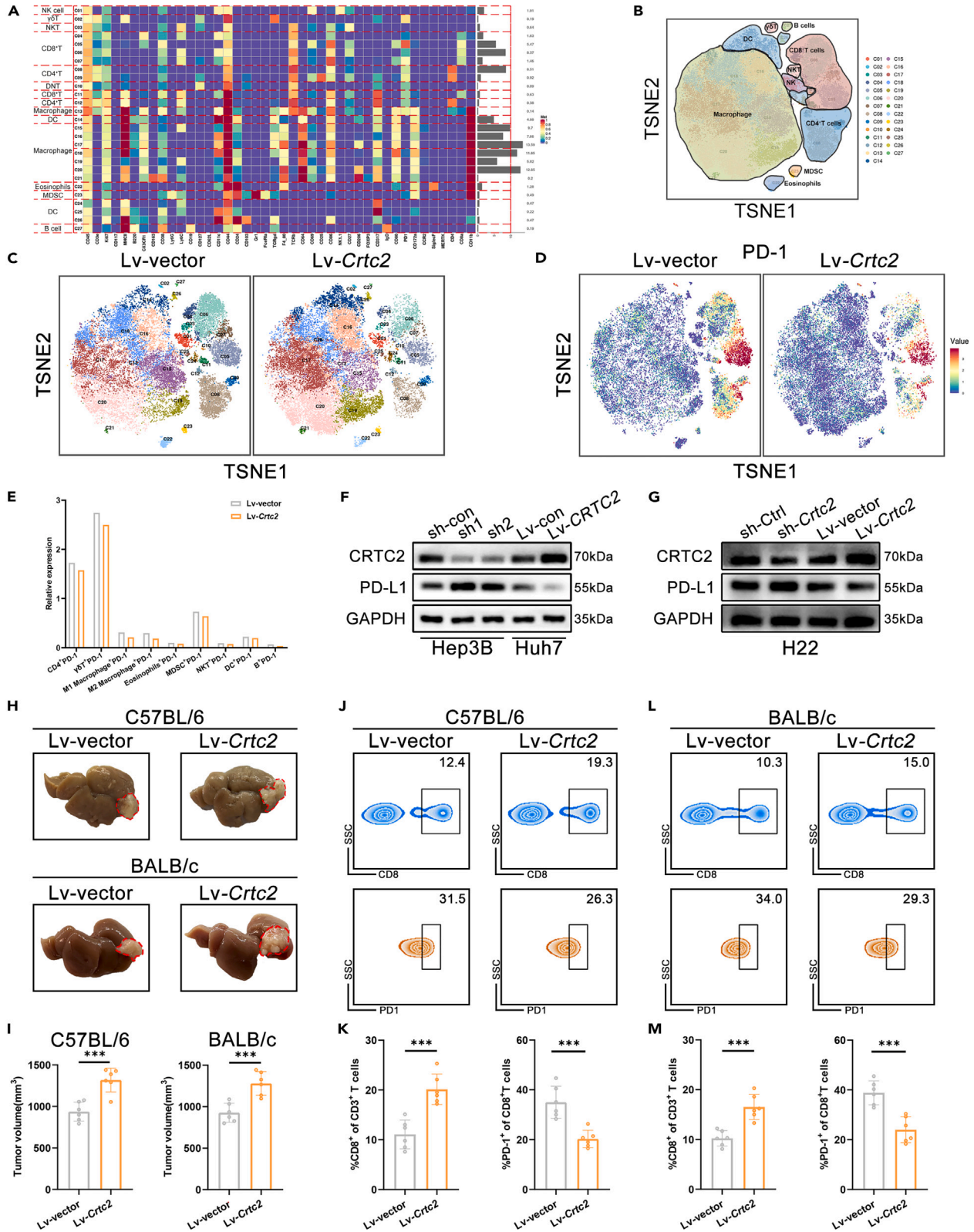
Figure 7. *Crtc2* downregulates the PD-L1/PD-1 axis

(A) There were 27 cell clusters in total, which were defined in the respective groups.

(B) The t-distributed stochastic neighbor embedding (t-SNE) plot showing the 27 major cell clusters.

(C) Distribution of 27 major cell clusters in each group, as shown by t-SNE plots.

(D) Distribution of PD-1$^+$ cell clusters in each group, as shown by t-SNE plots.

(E) Relative expression of PD-1$^+$ immune cells in each group.

(F and G) The protein expression of PD-L1 in transfected human HCC cells and mouse HCC cells.

(H) Representative orthotopic tumors collected from H22-bearing C57BL/6 (upper) and BALB/c mice (lower).

(I) Volume statistics of orthotopic tumors for each group, $n = 6$ per group.

(J and K) Flow cytometry analysis of CD8$^+$ in CD3$^+$ T cells and PD-1$^+$ in CD8$^+$ T cells from C57BL/6 orthotopic tumors and their quantitation, $n = 6$ per group.

(L and M) Flow cytometry analysis of CD8$^+$ in CD3$^+$ T cells and PD-1$^+$ in CD8$^+$ T cells from BALB/c orthotopic tumors and their quantitation, $n = 6$ per group. All data are presented as the mean $\pm$ SD, ** $p < 0.01$; *** $p < 0.001$.

LEF and TCF to form a transcriptional complex and increases the transcriptional activities of genes involved in proliferation, migration, and invasion, thus promoting distant metastasis and rapid progression of HCC.[32,33] Mechanistically, we confirmed that *CRTC2* overexpression upregulated TCF/LEF transcriptional activity, enhancing HCC malignant phenotypes. Besides, inhibition of the Wnt/β-catenin pathway reversed CRTC2-induced promotion of HCC malignant phenotypes. Therefore, we validated that *CRTC2* overexpression promotes HCC malignant phenotypes through the activated Wnt/β-catenin pathway. However, the transcription factor CREB, which is regulated by CRTC2, also drives HCC malignant progression.[37,38] Hence, we could not exclude the possibility that CREB may be involved in CRTC2-mediated HCC malignant phenotypes.

Immune checkpoints are produced by effector lymphocytes to prevent excessive immunological responses. The phenomenon of tumor and stromal cells producing corresponding ligands is a biological mechanism employed by malignancies to evade immune surveillance.[39,40] For instance, the cytotoxic activity of effector T cells is constrained by tumor cells, which use PD-L1 to interact with the PD-1 receptor, resulting in the exhaustion or impairment of effector T cells.[7,39,41] This interaction between checkpoint proteins and their ligands can be blocked by ICIs, thereby reactivating the antitumor effects of effector T cells, and enhancing immune surveillance. ICIs such as pembrolizumab have proven to be effective in patients with advanced HCC.[42] Despite the remarkable antitumor effects observed with ICIs in patients with advanced HCC, not all patients are sensitive to anti-PD-1 immunotherapy. Tumor-intrinsic properties, including mutational load, presentation of tumor antigens, or specific oncogenic pathways, can greatly influence antitumor immunity and response to immunotherapies. Hence, developing strategies to sensitize anti-PD-1 immunotherapy in patients with HCC is of utmost importance. Combination treatment of atezolizumab and bevacizumab effectively improved immunotherapy responsiveness in patients with unresectable HCC.[43] Considering the downregulation of PD-L1/PD-1 axis caused by *Crtc2* overexpression, we hypothesized that *Crtc2* knockdown may sensitize anti-PD-1 immunotherapy in HCC. As demonstrated by mouse subcutaneous and orthotopic HCC models, the combination therapy of *Crtc2* knockdown and anti-PD-1 synergistically restrained tumor growth, increased the tumor-infiltrating CD8$^+$ T cells, and notably upregulated the immunostimulatory cytokines. Our study provided evidence that targeting *Crtc2* enhanced the responsiveness to anti-PD-1 therapy in HCC.

In summary, we demonstrate that *CRTC2* drives HCC malignant phenotypes by activating the Wnt/β-catenin pathway. DNA promoter hypomethylation drives *CRTC2* upregulation in HCC. *Crtc2* facilitates tumor growth and drives primary resistance to immunotherapy by downregulating the PD-L1/PD-1 axis. Collectively, targeting *CRTC2* might be a promising therapeutic strategy to increase susceptibility to immunotherapy in patients with HCC.

Limitations of the study

Our study identified that *CRTC2* drives HCC malignant phenotypes by activating the Wnt/β-catenin pathway. However, RNA sequencing and KEGG analysis showed many signaling pathways correlated with CRTC2, and these pathways may also be involved in the oncogenic effect of CRTC2 on HCC malignant phenotypes.

STAR★METHODS

Detailed methods are provided in the online version of this paper and include the following:

- KEY RESOURCES TABLE
- RESOURCE AVAILABILITY
  - Lead contact
  - Materials availability
  - Data and code availability
- EXPERIMENTAL MODEL AND STUDY PARTICIPANT DETAILS
  - Patients and specimens
  - Cell culture
  - Mice
- METHOD DETAILS
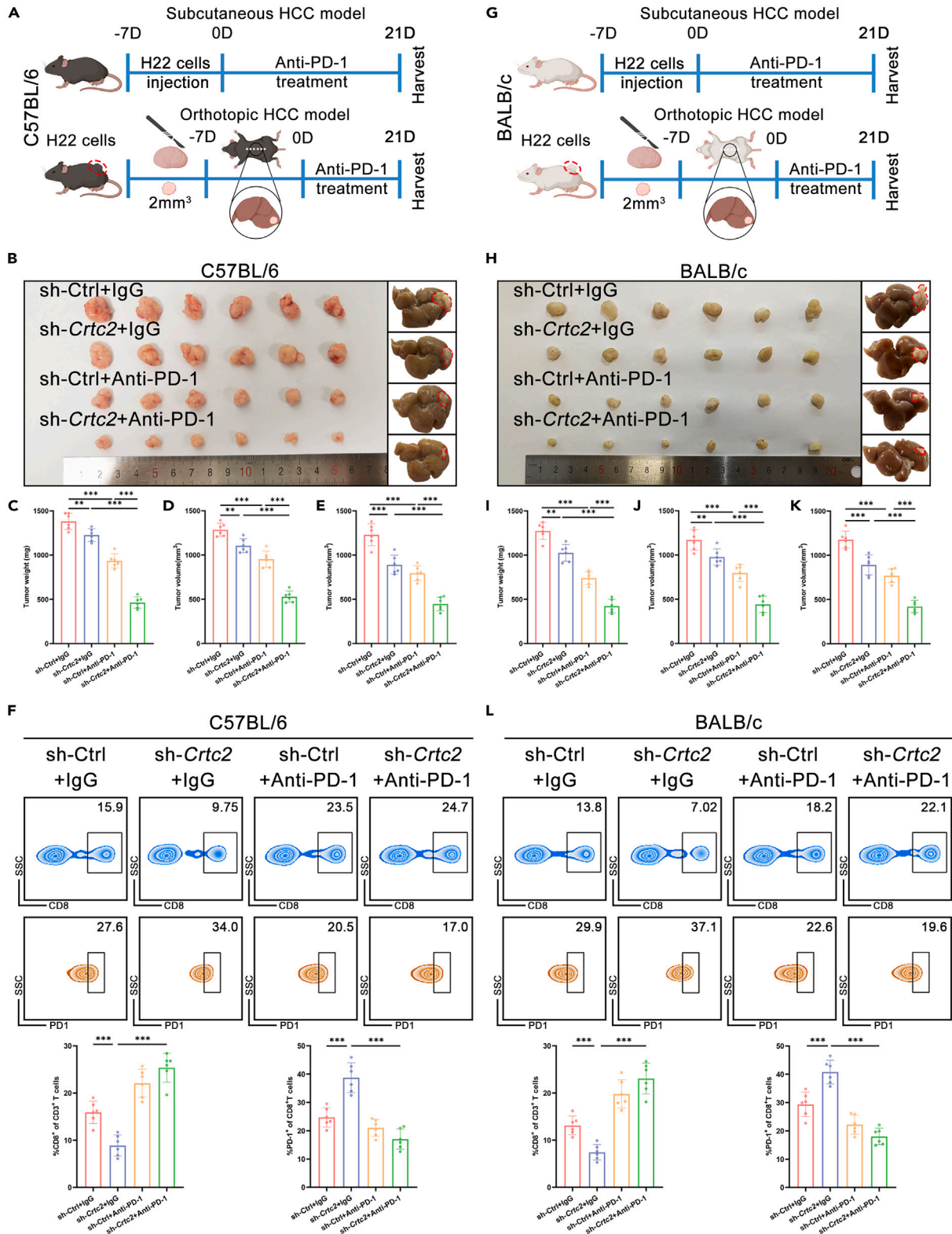
Figure 8. Targeting *Crtc2* sensitizes anti-PD-1 therapy in HCC

(A) Diagram showing the treatment strategy for subcutaneous tumors (upper) and orthotopic tumors (lower) in C57BL/6 mice.

(B) Photographs of the subcutaneous tumors (left) and orthotopic tumors (right), $n = 6$ per group.

(C and D) Weight and volume statistics of subcutaneous tumors, $n = 6$ per group.

(E) Volume statistics of orthotopic tumors, $n = 6$ per group.

(F) Flow cytometry analysis of $CD8^+$ in $CD3^+$ T cells and $PD-1^+$ in $CD8^+$ T cells from C57BL/6 orthotopic tumors and their quantitation, $n = 6$ per group.

(G) Diagram showing the treatment strategy for subcutaneous tumors (upper) and orthotopic tumors (lower) in BALB/c mice.

(H) Photographs of the subcutaneous tumors (left) and orthotopic tumors (right), $n = 6$ per group.

(I and J) Weight and volume statistics of subcutaneous tumors, $n = 6$ per group.

(K) Volume statistics of orthotopic tumors, $n = 6$ per group.

(L) Flow cytometry analysis of $CD8^+$ in $CD3^+$ T cells and $PD-1^+$ in $CD8^+$ T cells from BALB/c orthotopic tumors and their quantitation, $n = 6$ per group. All data are presented as the mean $\pm$ SD, $**p < 0.01$; $***p < 0.001$.

- ○ Antibodies and chemicals
- ○ Cell transfection and treatment
- ○ qRT-PCR
- ○ Western blotting
- ○ Methylation-specific PCR (MSP) analysis
- ○ Bisulfite sequencing PCR (BSP) analysis
- ○ Cell proliferation assays
- ○ Wound healing assays
- ○ Transwell assays
- ○ Apoptosis assays
- ○ Flow cytometry
- ○ Enzyme-linked immunosorbent assay (ELISA)
- ○ Animal studies
- ○ RNA sequencing analysis
- ○ Dual luciferase reporter assay
- ○ Immunohistochemistry (IHC)
- ○ Mass cytometry and data analysis
- ● QUANTIFICATION AND STATISTICAL ANALYSIS

SUPPLEMENTAL INFORMATION

Supplemental information can be found online at https://doi.org/10.1016/j.isci.2024.109821.

AUTHOR CONTRIBUTIONS

Q.L., Jing Xu, L.Z., and B.F. provided the experimental design and technical support. R.Z., J.D., F.Y., K.Y., and Y.C. performed the experiments. S.Z., W.H., and Jiali Xu performed the data analyses. R.Z. and J.D. wrote the manuscript. Q.L. organized and supervised the study.

DECLARATION OF INTERESTS

The authors declare no competing interests.

REFERENCES

1. Villanueva, A. (2019). Hepatocellular Carcinoma. N. Engl. J. Med. *380*, 1450–1462. https://doi.org/10.1056/NEJMra1713263.

2. Sung, H., Ferlay, J., Siegel, R.L., Laversanne, M., Soerjomataram, I., Jemal, A., and Bray, F. (2021). Global Cancer Statistics 2020: GLOBOCAN Estimates of Incidence and Mortality Worldwide for 36 Cancers in 185 Countries. CA Cancer J. Clin. *71*, 209–249. https://doi.org/10.3322/caac.21660.

3. Li, Q., Ni, Y., Zhang, L., Jiang, R., Xu, J., Yang, H., Hu, Y., Qiu, J., Pu, L., Tang, J., and Wang, X. (2021). HIF-1alpha-induced expression of m6A reader YTHDF1 drives hypoxia-induced autophagy and malignancy of hepatocellular carcinoma by promoting ATG2A and ATG14 translation. Signal Transduct. Target. Ther. *6*, 76. https://doi.org/10.1038/s41392-020-00453-8.

4. Huang, D.Q., El-Serag, H.B., and Loomba, R. (2021). Global epidemiology of NAFLD-related HCC: trends, predictions, risk factors and prevention. Nat. Rev. Gastroenterol. Hepatol. *18*, 223–238. https://doi.org/10.1038/s41575-020-00381-6.

5. Forner, A., Reig, M., and Bruix, J. (2018). Hepatocellular carcinoma. Lancet *391*, 1301–1314. https://doi.org/10.1016/S0140-6736(18)30010-2.

6. Xu, J., Zhang, L., Li, N., Dai, J., Zhang, R., Yao, F., Zhou, S., Wu, Z., Zhou, H., Zhou, L., et al. (2023). Etomidate elicits anti-tumor capacity by disrupting the JAK2/STAT3 signaling pathway in hepatocellular carcinoma. Cancer Lett. *552*, 215970. https://doi.org/10.1016/j.canlet.2022.215970.

7. Li, Q., Zhang, L., You, W., Xu, J., Dai, J., Hua, D., Zhang, R., Yao, F., Zhou, S., Huang, W., et al. (2022). PRDM1/BLIMP1 induces cancer immune evasion by modulating the USP22-SPI1-PD-L1 axis in hepatocellular carcinoma cells. Nat. Commun. *13*, 7677. https://doi.org/10.1038/s41467-022-35469-x.

8. Li, Q., Zhang, L., Yang, Q., Li, M., Pan, X., Xu, J., Zhong, C., Yao, F., Zhang, R., Zhou, S., et al. (2023). Thymidine kinase 1 drives hepatocellular carcinoma in enzyme-dependent and -independent manners. Cell Metabol. *35*, 912–927.e7. https://doi.org/10.1016/j.cmet.2023.03.017.

9. Li, Z., Wu, X., Zhao, Y., Xiao, Y., Zhao, Y., Zhang, T., Li, H., Sha, F., Wang, Y., Deng, L., and Ma, X. (2021). Clinical benefit of neoadjuvant anti-PD-1/PD-L1 utilization among different tumors. MedComm *2*, 60–68. https://doi.org/10.1002/mco2.61.

10. Zhang, L., Xu, J., Zhou, S., Yao, F., Zhang, R., You, W., Dai, J., Yu, K., Zhang, Y., Baheti, T., et al. (2024). Endothelial DGKG promotes tumor angiogenesis and immune evasion in hepatocellular carcinoma. J. Hepatol. *80*, 82–98. https://doi.org/10.1016/j.jhep.2023.10.006.

11. Gunasekaran, G., Bekki, Y., Lourdusamy, V., and Schwartz, M. (2021). Surgical Treatments of Hepatobiliary Cancers. Hepatology *73* (*Suppl 1*), 128–136. https://doi.org/10.1002/hep.31325.

12. Yu, M., Peng, Z., Qin, M., Liu, Y., Wang, J., Zhang, C., Lin, J., Dong, T., Wang, L., Li, S., et al. (2021). Interferon-gamma induces tumor resistance to anti-PD-1 immunotherapy by promoting YAP phase separation. Mol. Cell. *81*, 1216–1230.e9. https://doi.org/10.1016/j.molcel.2021.01.010.

13. Pinato, D.J., Fessas, P., Sapisochin, G., and Marron, T.U. (2021). Perspectives on the Neoadjuvant Use of Immunotherapy in Hepatocellular Carcinoma. Hepatology *74*, 483–490. https://doi.org/10.1002/hep.31697.

14. Papalexi, E., Mimitou, E.P., Butler, A.W., Foster, S., Bracken, B., Mauck, W.M., Wessels, H.H., Hao, Y., Yeung, B.Z., Smibert, P., and Satija, R. (2021). Characterizing the molecular regulation of inhibitory immune checkpoints with multimodal single-cell screens. Nat. Genet. *53*, 322–331. https://doi.org/10.1038/s41588-021-00778-2.

15. Llovet, J.M., Ricci, S., Mazzaferro, V., Hilgard, P., Gane, E., Blanc, J.F., de Oliveira, A.C., Santoro, A., Raoul, J.L., Forner, A., et al. (2008). Sorafenib in advanced hepatocellular carcinoma. N. Engl. J. Med. *359*, 378–390. https://doi.org/10.1056/NEJMoa0708857.

16. Kudo, M., Finn, R.S., Qin, S., Han, K.H., Ikeda, K., Piscaglia, F., Baron, A., Park, J.W., Han, G., Jassem, J., et al. (2018). Lenvatinib versus sorafenib in first-line treatment of patients with unresectable hepatocellular carcinoma: a randomised phase 3 non-inferiority trial. Lancet *391*, 1163–1173. https://doi.org/10.1016/S0140-6736(18)30207-1.

17. Bruix, J., Qin, S., Merle, P., Granito, A., Huang, Y.H., Bodoky, G., Pracht, M., Yokosuka, O., Rosmorduc, O., Breder, V., et al. (2017). Regorafenib for patients with hepatocellular carcinoma who progressed on sorafenib treatment (RESORCE): a randomised, double-blind, placebo-controlled, phase 3 trial. Lancet *389*, 56–66. https://doi.org/10.1016/S0140-6736(16)32453-9.

18. Sangro, B., Melero, I., Wadhawan, S., Finn, R.S., Abou-Alfa, G.K., Cheng, A.L., Yau, T., Furuse, J., Park, J.W., Boyd, Z., et al. (2020). Association of inflammatory biomarkers with clinical outcomes in nivolumab-treated patients with advanced hepatocellular carcinoma. J. Hepatol. *73*, 1460–1469. https://doi.org/10.1016/j.jhep.2020.07.026.

19. Yang, W., Feng, Y., Zhou, J., Cheung, O.K.W., Cao, J., Wang, J., Tang, W., Tu, Y., Xu, L., Wu, F., et al. (2021). A selective HDAC8 inhibitor potentiates antitumor immunity and efficacy of immune checkpoint blockade in hepatocellular carcinoma. Sci. Transl. Med. *13*, eaaz6804. https://doi.org/10.1126/scitranslmed.aaz6804.

20. Tang, W., Chen, Z., Zhang, W., Cheng, Y., Zhang, B., Wu, F., Wang, Q., Wang, S., Rong, D., Reiter, F.P., et al. (2020). The mechanisms of sorafenib resistance in hepatocellular carcinoma: theoretical basis and therapeutic aspects. Signal Transduct. Targeted Ther. *5*, 87. https://doi.org/10.1038/s41392-020-0187-x.

21. Altarejos, J.Y., and Montminy, M. (2011). CREB and the CRTC co-activators: sensors for hormonal and metabolic signals. Nat. Rev. Mol. Cell Biol. *12*, 141–151. https://doi.org/10.1038/nrm3072.

22. Shaywitz, A.J., and Greenberg, M.E. (1999). CREB: a stimulus-induced transcription factor activated by a diverse array of extracellular signals. Annu. Rev. Biochem. *68*, 821–861. https://doi.org/10.1146/annurev.biochem.68.1.821.

23. Conkright, M.D., Canettieri, G., Screaton, R., Guzman, E., Miraglia, L., Hogenesch, J.B., and Montminy, M. (2003). TORCs: transducers of regulated CREB activity. Mol. Cell. *12*, 413–423. https://doi.org/10.1016/j.molcel.2003.08.013.

24. Wang, Y., Vera, L., Fischer, W.H., and Montminy, M. (2009). The CREB coactivator CRTC2 links hepatic ER stress and fasting gluconeogenesis. Nature *460*, 534–537. https://doi.org/10.1038/nature08111.

25. Koo, S.H., Flechner, L., Qi, L., Zhang, X., Screaton, R.A., Jeffries, S., Hedrick, S., Xu, W., Boussouar, F., Brindle, P., et al. (2005). The CREB coactivator TORC2 is a key regulator of fasting glucose metabolism. Nature *437*, 1109–1111. https://doi.org/10.1038/nature03967.

26. Han, H.S., Kim, S.G., Kim, Y.S., Jang, S.H., Kwon, Y., Choi, D., Huh, T., Moon, E., Ahn, E., Seong, J.K., et al. (2022). A novel role of CRTC2 in promoting nonalcoholic fatty liver disease. Mol. Metabol. *55*, 101402. https://doi.org/10.1016/j.molmet.2021.101402.

27. Fang, M., Pak, M.L., Chamberlain, L., Xing, W., Yu, H., and Green, M.R. (2015). The CREB Coactivator CRTC2 Is a Lymphoma Tumor Suppressor that Preserves Genome Integrity through Transcription of DNA Mismatch Repair Genes. Cell Rep. *11*, 1350–1357. https://doi.org/10.1016/j.celrep.2015.04.052.

28. Rodon, L., Svensson, R.U., Wiater, E., Chun, M.G.H., Tsai, W.W., Eichner, L.J., Shaw, R.J., and Montminy, M. (2019). The CREB coactivator CRTC2 promotes oncogenesis in LKB1-mutant non-small cell lung cancer. Sci. Adv. *5*, eaaw6455. https://doi.org/10.1126/sciadv.aaw6455.

29. Lee, H., Lee, M., and Hong, S.K. (2019). CRTC2 as a novel prognostic biomarker for worse pathologic outcomes and biochemical recurrence after radical prostatectomy in patients with prostate cancer. Investig. Clin. Urol. *60*, 84–90. https://doi.org/10.4111/icu.2019.60.2.84.

30. Wang, Y., Liu, Q., and Zhang, H. (2020). Phosphorylation of CREB-Specific Coactivator CRTC2 at Ser238 Promotes Proliferation, Migration, and Invasion of Colorectal Cancer Cells. Technol. Cancer Res. Treat. *19*, 1533033820962111. https://doi.org/10.1177/1533033820962111.

31. Ahn, H.R., Baek, G.O., Yoon, M.G., Son, J.A., Yoon, J.H., Cheong, J.Y., Cho, H.J., Kang, H.C., Eun, J.W., and Kim, S.S. (2022). Hypomethylation-mediated upregulation of the WASF2 promoter region correlates with poor clinical outcomes in hepatocellular carcinoma. J. Exp. Clin. Cancer Res. *41*, 158. https://doi.org/10.1186/s13046-022-02365-7.

32. Xu, C., Xu, Z., Zhang, Y., Evert, M., Calvisi, D.F., and Chen, X. (2022). beta-Catenin signaling in hepatocellular carcinoma. J. Clin. Invest. *132*, e154515. https://doi.org/10.1172/JCI154515.

33. Perugorria, M.J., Olaizola, P., Labiano, I., Esparza-Baquer, A., Marzioni, M., Marin, J.J.G., Bujanda, L., and Banales, J.M. (2019). Wnt-beta-catenin signalling in liver development, health and disease. Nat. Rev. Gastroenterol. Hepatol. *16*, 121–136. https://doi.org/10.1038/s41575-018-0075-9.

34. Huang, S.M.A., Mishina, Y.M., Liu, S., Cheung, A., Stegmeier, F., Michaud, G.A., Charlat, O., Wiellette, E., Zhang, Y., Wiessner, S., et al. (2009). Tankyrase inhibition stabilizes axin and antagonizes Wnt signalling. Nature *461*, 614–620. https://doi.org/10.1038/nature08356.

35. Stefanska, B., Cheishvili, D., Suderman, M., Arakelian, A., Huang, J., Hallett, M., Han, Z.G., Al-Mahtab, M., Akbar, S.M.F., Khan, W.A., et al. (2014). Genome-wide study of hypomethylated and induced genes in patients with liver cancer unravels novel anticancer targets. Clin. Cancer Res. *20*, 3118–3132. https://doi.org/10.1158/1078-0432.CCR-13-0283.

36. Calvisi, D.F., Ladu, S., Gorden, A., Farina, M., Lee, J.S., Conner, E.A., Schroeder, I., Factor, V.M., and Thorgeirsson, S.S. (2007). Mechanistic and prognostic significance of aberrant methylation in the molecular pathogenesis of human hepatocellular carcinoma. J. Clin. Invest. *117*, 2713–2722. https://doi.org/10.1172/JCI31457.

37. Sapio, L., Salzillo, A., Ragone, A., Illiano, M., Spina, A., and Naviglio, S. (2020). Targeting CREB in Cancer Therapy: A Key Candidate or One of Many? An Update. Cancers *12*, 3166. https://doi.org/10.3390/cancers12113166.

38. Zhang, T., Zhang, J., You, X., Liu, Q., Du, Y., Gao, Y., Shan, C., Kong, G., Wang, Y., Yang, X., et al. (2012). Hepatitis B virus X protein modulates oncogene Yes-associated protein by CREB to promote growth of hepatoma cells. Hepatology *56*, 2051–2059. https://doi.org/10.1002/hep.25899.

39. He, X., and Xu, C. (2020). Immune checkpoint signaling and cancer immunotherapy. Cell Res. *30*, 660–669. https://doi.org/10.1038/s41422-020-0343-4.

40. Chen, L., and Flies, D.B. (2013). Molecular mechanisms of T cell co-stimulation and co-inhibition. Nat. Rev. Immunol. *13*, 227–242. https://doi.org/10.1038/nri3405.

41. Pardoll, D.M. (2012). The blockade of immune checkpoints in cancer immunotherapy. Nat. Rev. Cancer *12*, 252–264. https://doi.org/10.1038/nrc3239.

42. Zhu, A.X., Finn, R.S., Edeline, J., Cattan, S., Ogasawara, S., Palmer, D., Verslype, C., Zagonel, V., Fartoux, L., Vogel, A., et al. (2018). Pembrolizumab in patients with advanced hepatocellular carcinoma previously treated with sorafenib (KEYNOTE-224): a non-randomised, open-label phase 2 trial. Lancet Oncol. *19*, 940–952. https://doi.org/10.1016/S1470-2045(18)30351-6.

43. Finn, R.S., Qin, S., Ikeda, M., Galle, P.R., Ducreux, M., Kim, T.Y., Kudo, M., Breder, V., Merle, P., Kaseb, A.O., et al. (2020). Atezolizumab plus Bevacizumab in Unresectable Hepatocellular Carcinoma. N. Engl. J. Med. *382*, 1894–1905. https://doi.org/10.1056/NEJMoa1915745.

STAR★METHODS

KEY RESOURCES TABLE

REAGENT or RESOURCE	SOURCE	IDENTIFIER
Antibodies		
Anti-CRTC2, dil:1/1000	Proteintech	Cat# 12497-1-AP; RRID:AB_2260910
Anti-CRTC2, dil:1/100	Abcam	Cat# Ab109081; RRID:AB_10859591
Anti-WASF2, dil:1/1000	Cell Signaling Technology	Cat# 3659; RRID:AB_2216981
Anti-CyclinD1, dil:1/40000	Proteintech	Cat# 60186-1-Ig; RRID:AB_10793718
Anti-CD44, dil:1/6000	Proteintech	Cat# 15675-1-AP; RRID:AB_2076198
Anti-c-Met, dil:1/5000	Proteintech	Cat# 25869-1-AP; RRID:AB_2880276
Anti-c-Jun, dil:1/1000	Cell Signaling Technology	Cat# 9165; RRID:AB_2130165
Anti-TCF-1, dil: 1:1000	Cell Signaling Technology	Cat# 2203; RRID:AB_2199302
Anti-PD-L1, dil:1/5000	Proteintech	Cat# 66248-1-Ig; RRID:AB_2756526
Anti-GAPDH, dil:1/5000	Proteintech	Cat# 60004-1-Ig; RRID:AB_2107436
BD Fc block, dil:1/150	Biosciences	Cat# 553142; RRID:AB_394656
Anti-mouse CD3, dil:1/100	BioLegend	Cat# 100220; RRID:AB_1732068
Anti-mouse CD8a, dil:1/100	BioLegend	Cat# 162306; RRID:AB_2927947
Anti-mouse PD-1, dil:1/100	BioLegend	Cat# 135223; RRID:AB_2563522
Goat anti-mouse IgG (H + L), dil:1/5000	Jackson	Cat# 115-035-003; RRID: AB_10015289
Goat anti-rabbit IgG (H + L), dil:1/5000	Jackson	Cat# 111-035-003; RRID: AB_2313567
Bacterial and virus strains		
Lentivirus CRTC2 overexpression	GENECHEM	N/A
Lentivirus shCRTC2	GENECHEM	N/A
Plasmid TOP-Flash reporter	This paper	N/A
Plasmid CRTC2 control	This paper	N/A
Plasmid CRTC2 overexpression	This paper	N/A
Biological samples		
HCC tissues	The First Affiliated Hospital of Nanjing Medical University	N/A
HCC tissues microarray	The First Affiliated Hospital of Nanjing Medical University	N/A
Chemicals, peptides, and recombinant proteins		
RIPA buffer	Beyotime	Cat# P0013B
XAV-939	Abcam	Cat# Ab120897
Triton X-100	Sigma-Aldrich	Cat# T8787
Trypsin	GIBCO	Cat# 27250-018
DAPI	Invitrogen	Cat# S36939
Penicillin-Streptomycin	GIBCO	Cat# 15140-122
FBS	Bio-One Biotechnology	Cat# F05-001-B160216
Puromycin	Sigma-Aldrich	Cat# 58-58-2
PBS	WISENT	Cat# 311-010-CL
IgG isotype	Bio X cell	Cat# BE0089
Anti-PD-1	Bio X cell	Cat# BE0146
D-luciferin	Beyotime	Cat# ST196
Fixable Viability Stain 620	Biosciences	Cat# 564996

(Continued on next page)

Continued

REAGENT or RESOURCE	SOURCE	IDENTIFIER
DMEM	WISENT	Cat# 319-005-CL
5-Aza-dC	Sigma-Aldrich	Cat# 2353-33-5
Critical commercial assays		
BCA protein assay kit	Thermo Fisher	Cat# 23225
Annexin V-FITC/PI Apoptosis Detection Kit	Vazyme	Cat# A211-01/02
EdU kit	Beyotime	Cat# C0078S
RNA Rapid Extraction Kit	Thermo Fisher	Cat# AM9775
HiScript III RT SuperMix for qPCR	Vazyme	Cat# R323-01
ChamQ SYBR® qPCR Master Mix	Vazyme	Cat# Q341-02
Lipofectamine 3000	Invitrogen	Cat# L3000015
ECL kit	Beyotime	Cat# P0018M
Dual Luciferase Reporter Gene Assay Kit	Beyotime	Cat# RG027
Methylation-Gold Kit	Zymo Research	Cat# D5006
TGF-beta ELISA Kit	R&D systems	Cat# DB100C
IFN-gamma ELISA Kit	R&D systems	Cat# MIF00
TNF-alpha ELISA Kit	R&D systems	Cat# MTA00B
IL-10 ELISA Kit	R&D systems	Cat# M1000B
TIANamp Genomic DNA Kit	TIANGEN Biotech	Cat# DP304-03
Cell Counting Kit-8	MCE	Cat# HY-K0301
Deposited data		
RNA sequencing data	This paper	HRA007128
Experimental models: Cell lines		
MIHA	American Type Culture Collection	N/A
Hep3B	Cell bank of CAS	N/A
Huh7	Cell bank of CAS	N/A
HLF	Japanese Cancer Research Resources Bank	Cat# JCRB0405
MHCC97L	Cell bank of CAS	N/A
HCCLM3	Cell bank of CAS	N/A
H22	China Center for Type Culture Collection	N/A
Experimental models: Organisms/strains		
BALB/c nude male mouse	Vital River Laboratory	N/A
BALB/c male mouse	Vital River Laboratory	N/A
C57BL/6 male mouse	Vital River Laboratory	N/A
Oligonucleotides		
Primers for qRT-PCR, see Table S3	This paper	N/A
Target sequences for knockdown CRTC2, see Table S4	This paper	N/A
Primers for MSP, see Table S5	This paper	N/A
Primers for BSP, see Table S6	This paper	N/A
Software and algorithms		
Prism 10.0	GraphPad	N/A
ImageJ	Open source	N/A
SPSS statistics 22.0	IBM Corp	N/A
Quantification tool for Methylation Analysis	Open source	N/A
MethPrimer 2.0	Open source	N/A
cBioPortal	Open source	N/A

RESOURCE AVAILABILITY

Lead contact

Further information and requests for resources and reagents should be directed to the Lead Contact, Qing Li (liqingjsph@njmu.edu.cn).

Materials availability

No novel materials were produced and involved in this study.

Data and code availability

- The raw data reported in this paper have been deposited in the Genome Sequence Archive in National Genomics Data Center, China National Center for Bioinformation/Beijing Institute of Genomics, Chinese Academy of Sciences (GSA-Human: HRA007128 for RNA-seq data) that are publicly accessible at https://ngdc.cncb.ac.cn/gsa-human.
- This paper does not report original code.
- Any additional information required to reanalyze the data reported in this paper is available from the lead contact upon request.

EXPERIMENTAL MODEL AND STUDY PARTICIPANT DETAILS

Patients and specimens

HCC tissues and matched adjacent normal tissues were collected from February 2013 to March 2016 at the First Affiliated Hospital, Nanjing Medical University. None of these patients had received interventional therapy, chemotherapy, or radiotherapy before partial hepatectomy. Immediately after removal, tumor tissues and adjacent normal liver tissues were frozen in liquid nitrogen or fixed with 4% paraformaldehyde (PFA), and two well-experienced pathologists evaluated each sample and scored it based on histological and pathological findings. The clinicopathological information of patients with HCC in this study is presented in Tables S1 and S2. This study was approved by the Ethics Committee of the First Affiliated Hospital of Nanjing Medical University, and written informed consent was signed by all patients.

Cell culture

Immortalized liver cell line (MIHA) was obtained from American Type Culture Collection (ATCC). Human HCC cell lines (Hep3B, Huh7, MHCC97L, and HCCLM3) were obtained from the Shanghai Institutes for Biological Sciences, Chinese Academy of Sciences (CAS). HLF cell line was obtained from Japanese Cancer Research Resources Bank (JCRB). H22 cell line was purchased from China Center for Type Culture Collection (CCTCC). Cells were cultivated and grown in DMEM supplied with 10% FBS (Gibico, USA) and 1% penicillin/streptomycin at 37°C in a humidified incubator with 5% CO_2.

Mice

4-week-old BALB/c nude male mice, 4-week-old C57BL/6 male mice and 4-week-old BALB/c male mice were purchased from Beijing Vital River Laboratory Animal Technologies. Mice were group housed in specific pathogen free (SPF) conditions, dark/light cycles: 12-h light/12-h dark (150–300 lux), ambient temperature 20°C–26°C and humidity 40%–70%, ventilated four times per hour. Mice were randomly distributed into different groups by body weight and fed with standard chow diet. All animal experiments were approved by the Institutional Animal Care and Use Committee (IACUC) of Nanjing Medical University (Approval Code: 2304040).

METHOD DETAILS

Antibodies and chemicals

The following antibodies were chosen for western blotting: Anti-CRTC2, dil:1/1000 (12497-1-AP, Proteintech, China); Anti-WASF2, dil:1/1000 (3659, Cell signaling Technology, China); Anti-CyclinD1, dil:1/40000 (60186-1-Ig, Proteintech); Anti-CD44, dil:1/6000 (15675-1-AP, Proteintech); Anti-c-Met, dil:1/5000 (25869-1-AP, Proteintech); Anti-c-Jun, dil:1/1000 (9165, Cell signaling Technology); Anti-TCF-1, dil: 1:1000 (2203, Cell signaling Technology); Anti-PD-L1, dil:1/5000 (66248-1-Ig, Proteintech); Anti-GAPDH, dil:1/5000 (60004-1-Ig, Proteintech); Goat anti-mouse IgG (H + L) (115-035-003, 1:5000) and Goat anti-rabbit IgG (H + L) (111-035-003, 1:5000) were purchased from Jackson (USA). The following chemicals were used for cell pretreatment: XAV-939 (Ab120897, Abcam, UK); 5-Aza-dC (2353-33-5, Sigma-Aldrich, USA).

Cell transfection and treatment

GeneChem (Shanghai, China) was employed to design and fabricate specific lentiviral vectors. These vectors consisted of empty vectors, target genes, and short hairpin RNAs (shRNAs). Table S4 contains the sequences of different shRNAs used. After transfection, stable cell lines were selected by cultivating them with puromycin (58-58-2, Sigma-Aldrich) at a concentration of 5 μg/mL for 7 days. To inhibit the activity of Wnt/β-catenin pathway, XAV-939 was diluted at a concentration of 1 μmol in dimethyl sulfoxide (DMSO). To confirm the impact of DNA methylation on CRTC2 expression, Hep3B and Huh7 cells were diluted to a confluence level of only 50% and exposed to 2 μM 5-Aza-dC for 4 days.

qRT-PCR

Per the manufacturer's instructions, total RNA was extracted and purified using the RNA Rapid Extraction Kit (AM9775, Thermo Fisher, USA). Thereafter, cDNA was synthesized by PrimeScript RT Reagent kit (R323-01, Vazyme, China) and qRT-PCR was conducted using the SYBR Green PCR kit (Q341-02, Vazyme). The primer sequences involved in qRT-PCR are listed in Table S3. β-actin was considered as an endogenous gene. The $2^{-\Delta Ct}$ method was used to calculate the relative mRNA expression.

Western blotting

Total protein from HCC tissues, matched adjacent normal tissues, and cell lines was extracted on ice by RIPA (P0013B, Beyotime, China). Further, proteins were separated by 10% SDS-PAGE (Beyotime) and subsequently transferred onto PVDF membranes. The membranes were incubated with the corresponding primary antibodies at 4°C overnight, washed thrice by PBS, and incubated with HRP-conjugated secondary antibodies for 2 h. ECL signals of the PVDF membranes were detected by an ECL kit containing BeyoECL Plus A and B (P0018M, Beyotime). GAPDH was used as an endogenous gene.

Methylation-specific PCR (MSP) analysis

In accordance with the manufacturer's guidelines, genomic DNA was extracted from HCC cells utilizing the TIANamp Genomic DNA Kit (DP304-03, TIANGEN Biotech, China). DNA was subjected to sodium bisulfite treatment using the Methylation-Gold Kit (D5006, Zymo Research, USA). Table S5 lists forward and reverse primers for the methylation (M) and the unmethylation (U) sequences.

Bisulfite sequencing PCR (BSP) analysis

The Methylation-Gold kit was used for bisulfite treatment of the extracted genomic DNA under the manufacturer's instructions. The online bioinformatics analysis website MethPrimer 2.0 was employed to identify the potential CpG islands of CRTC2 -2000 bp to +1000 bp from the transcription start site (NC_000001.11:c153960612-153957612) and design specific primers for quantitative methylation analysis. Using BSP primers, we amplified the bisulfite-treated genomic DNA. PCR products were cloned into pMD19-T (TaKaRa) after purification. DNA sequencing was performed using the cloned products. Primers used for BSP are shown in Table S6.

Cell proliferation assays

For the CCK-8 assays, HCC cells were cultured in a 96-well plate. A fixed amount of CCK-8 solution (HY-K0301, MCE, USA) was added to each well at the indicated time points and incubated for 2 h at 37°C. Multiskan GO (Thermo Fisher) was used to measure the absorbance of the cells at 450 nm. For colony formation assays, HCC cells were seeded in a 6-well plate and cultured in 2 mL of medium for 10–14 days. The proliferating colonies were then fixed with alcohol and stained with crystal violet. Finally, the visible colonies were photographed and counted. For EdU assays, transfected HCC cells were seeded in a 12-well plate and cultured overnight. Next, 50 μM 5-Ethynyl-2′-deoxyuridine (C0078S, Beyotime) was added to each well, and the plate was incubated at 37°C for 2 h. The cells were then fixed, permeabilized, and treated with 400 μL of Hoechst 33342 to stain the nucleus. The number of cells in five randomly selected areas of each well was counted to determine the proportion of EdU-positive cells.

Wound healing assays

Transfected HCC cells were seeded in 6-well plates. When cells were grown to 80% confluence, an artificial wound was made using a 200 μL pipette tip. The wound was imaged at the same spot at 0 and 24 h (s1 and s2), and the relative cell mobility was calculated using the formula: (s1-s2)/s1 × 100%.

Transwell assays

The upper chamber of a transwell plate was loaded with 200 μL serum-free medium containing 1×10^4 cells, and the lower chamber was loaded with 800 μL serum-containing medium. After 24 h, cells remaining in the upper chamber were gently washed away with PBS, and the migrating cells were fixed in 4% PFA for 15 min. After fixation, cells were stained with crystal violet (Beyotime) for 30 min. The labeled cells were then photographed and counted using an inverted optical microscope. For the invasion assay, Matrigel was added to the plate surface to explore the invasive ability of the cells.

Apoptosis assays

After incubation in serum-free medium for 24 h, HCC cells were resuspended in ice-cold PBS and incubated at 37°C for 20 min with FITC Annexin V and PI staining solution (A211-01/02, Vazyme). The cells were then subjected to flow cytometry and analyzed by FlowJo software.

Flow cytometry

Freshly resected mouse orthotopic tumors were collected, cut into 50–100 mm³, and dispersed into single cell suspensions. Cells were incubated with BD Fc block (553142, Biosciences, USA) for 30 min on ice, followed by incubation with relevant antibodies for 30 min on ice,

including PE-CD3, APC-CD8, Cyanine7-PD-1 (BioLegend, USA). Dead cells were excluded using the Fixable Viability Dye (Biosciences). Cells were then washed thrice by PBS and subjected to flow cytometry. Gating strategy used for flow cytometry staining was provided in Figure S4.

Enzyme-linked immunosorbent assay (ELISA)

Tumor lysates were collected and analyzed to quantify cytokines release induced by the interaction between immune cells and tumors. ELISA were performed using relevant ELISA kits IL-10 (M1000B, R&D systems, USA), IFN-γ (MIF00, R&D systems), TNF-α (MTA00B, R&D systems), TGF-β (DB100C, R&D systems) according to the manufacturer's instructions.

Animal studies

To evaluate the impact of CRTC2 on HCC malignant phenotypes *in vivo*, 1×10^6 transfected HCC cells resuspended in PBS were subcutaneously injected into 4-week-old male nude mice. Tumor size was measured and recorded once a week. The tumor volume was calculated as (width^2 × length)/2. For lung metastasis assays, HCC cells (1×10^6 cells/100 μL PBS) were injected into 4-week-old male nude mice via the tail vein. Four weeks later, the mice were intraperitoneally injected with 100 mg/kg D-luciferin (ST196, Beyotime), and corresponding luminescence was detected using the IVIS Lumina Imaging System (Xenogen). For the establishment of immunocompetent HCC subcutaneous model, mouse HCC cells were subcutaneously injected into 4-week-old male C57BL/6 or BALB/c mice. For the establishment of immune-competent HCC orthotopic model, subcutaneous tumors from tumor-bearing C57BL/6 or BALB/c mice were isolated, cut into 1–2 mm^3 pieces, and transplanted into the incision of liver lobe. Immunotherapy was initiated on the 7th day after the establishment of subcutaneous and orthotopic tumor models, each group received an intraperitoneal injection of 200 μg mouse anti-PD-1 (BE0146, Bio X cell, USA) or IgG isotype control (BE0089, Bio X cell), and these injections were repeated every three days. All mice were observed every 3 days and sacrificed on day 21 to examine the synergistic effect of CRTC2 knockdown and anti-PD-1 treatment.

RNA sequencing analysis

Total RNA was extracted from HCC cells using RNA Rapid Extraction Kit (AM9775, Thermo Fisher), and the corresponding cDNA library was constructed. Subsequently, a single-end sequencing library was generated from the samples using a BGISEQ500 instrument. Differently expressed genes whose expression was upregulated by more than 2.0-fold were identified and subjected to the KEGG pathway enrichment analysis.

Dual luciferase reporter assay

To evaluate the effect of *CRTC2* dysregulation on the transcriptional activity of TCF/LEF, the TOP-Flash reporter plasmid, control plasmid, and *CRTC2* overexpression plasmid were transiently co-transfected into HCC cells using Lipofectamine 3000 (L3000015, Invitrogen). *Renilla* luciferase vector plasmids were used as an internal control. After the collection of lysates from HCC cells, the luciferase activity of these groups was detected by a commercial Dual Luciferase Reporter Assay Kit (RG027, Beyotime).

Immunohistochemistry (IHC)

The levels of CRTC2 protein expression in clinical samples were assessed by IHC-score, which was calculated based on the percentage of stained cells and staining intensity (intensity of the staining was assessed on a scale of 0–3: 0, no staining; 1, weak staining; 2, moderate staining; 3, strong staining and the percentage of stained cells was assessed on a scale of 0–4: 0, 0%; 1, 1–24%; 2, 25–49%; 3, 50–74%; 4, 75–100%). The final IHC score was calculated by multiplying the positive staining rate and the positive staining area score.

Mass cytometry and data analysis

In brief, cells were stained with 250 nM Cisplatin-194Pt (Fluidigm, China) and then incubated in an Fc receptor blocking solution on ice. After washed thrice by PBS, the cells were subjected to staining with a surface antibodies cocktail for 30 min on ice before overnight incubation with DNA-staining 191/193Ir. After permeabilization, each sample was resuspended with an intracellular antibody staining cocktail and incubated on ice for 30 min. Further, cells were rinsed, and diluted in ddH$_2$O containing 20% EQ beads (Fluidigm) and analyzed by a mass cytometer (Helios, Fluidigm). Individual fully functional CD45$^+$ immune cells were gated, identified, and analyzed using FlowJo. Cell subpopulations were clustered and manually annotated using the X-shift algorithm. To visualize high-dimensional cell populations in two dimensions, the t-SNE algorithm was applied to represent the characteristics of the annotated cell populations and identify biomarkers.

QUANTIFICATION AND STATISTICAL ANALYSIS

Statistical analyses were conducted using SPSS Statistics (version 22.0, SPSS, NY, USA) and GraphPad Prism 10.0 (GraphPad Software, CA, USA). The Student's t test was used to evaluate the differences between two groups. Pearson's correlation test was used to evaluate the correlation between CRTC2 and DNA methylation levels. The correlations between CRTC2 expression and clinicopathological characteristics of patients with HCC were determined using the chi-square test. OS and DFS were analyzed using Kaplan-Meier analysis. All data were recorded as means ± standard deviation (SD), $*p < 0.05$; $**p < 0.01$; $***p < 0.001$; ns, not significant.